



In the quest for ionic liquid entrainers for the recovery of R-32 and R-125 by extractive distillation under rate-based considerations

Miguel Viar, Salvador Asensio-Delgado, Fernando Pardo, Gabriel Zarca^{*}, Ane Urtiaga^{*}

Department of Chemical and Biomolecular Engineering, Universidad de Cantabria, Av. Los Castros 46, 39005 Santander, Spain

ARTICLE INFO

Keywords:

Azeotropic separation
Extractive distillation
Hydrofluorocarbon
Ionic liquids
Refrigerant
R-410A

ABSTRACT

In line with the reduction targets imposed on the production of high global warming potential (GWP) hydrofluorocarbons by the Kigali Amendment to the Montreal Protocol, the recovery of refrigeration fluids at the end-of-life of refrigeration and air-conditioning equipment and the selective separation of the most valuable refrigerants is sought for recycling purposes and climate change mitigation. To that end, extractive distillation (ED) processes using ionic liquids (ILs) as entrainers is considered a promising technology to solve the difficulty of separating the typical close boiling or azeotropic behaviour of fluorinated hydrocarbon mixtures. This work provides insight into the design of ED processes evaluating the influence of both mass transfer phenomena (rate-based models) and IL properties (absorption capacity, solubility selectivity and viscosity) on the critical process variables (e.g., solvent-to-feed ratio, reboiler temperature, packing height) to separate the components of the binary mixture R-410A (50 wt% difluoromethane (R-32) + 50 wt% pentafluoroethane (R-125)) with minimum energy consumption and purity greater than 99.5 wt% of the two products. Results point to the solubility selectivity as the most influential IL property, and to $[C_2C_1im][SCN]$, among all ILs assessed, as a promising entrainer because of its high R-32/R-125 solubility selectivity and low viscosity, which enables to operate the ED process at lower temperatures. The recovered R-32 can be used as a greener alternative to the high-GWP R-410A, as well as a main component in the formulation of new low-GWP mixtures.

1. Introduction

Nowadays, the refrigeration market is suffering drastic changes aimed at reducing fabrication and use of high-global warming potential (GWP) hydrofluorocarbons (HFCs), which are employed massively in refrigeration and air-conditioning (RAC). Considering that the emissions of HFCs and related compounds account for 3% of the total greenhouse gas emissions and that incineration remains as the main end-of-life treatment, intense efforts are crucial to change the roadmap of the RAC sector [1]. Measures taken to avoid the atmospheric emissions of HFCs include the substitution of high-GWP HFCs by low-GWP hydrofluoroolefins (HFOs), and the reclamation of moderate-GWP HFCs from end-of-use RAC equipment.

The reprocessing of used refrigerants typically involves the separation of the components of the refrigerant mixture to meet the purity specifications as well as the technical, environmental and safety standards for new refrigerants. However, a majority of the installed RAC equipment is furnished with refrigerant fluids that are azeotropic or close-boiling mixtures of several HFCs, among others [2]. This

phenomenon renders conventional separation processes ineffective, leading to focus the research on three different advanced separation technologies: adsorption on porous materials [3–6], membrane separation processes [7–10], and absorption in liquid entrainers to perform extractive distillation (ED) processes [11–14].

The performance of ED is highly dependent on the properties of the liquid entrainer, which should exhibit several properties such as non-volatility, nonflammability, chemical and thermal stability, large liquid range, and tunable polarity [14]. In this regard, ionic liquids (ILs) [15,16] and, to a lesser extent, deep eutectic solvents [17,18] are being investigated as entrainers for ED processes because they can provide outstanding gas absorption capacity coupled with high solubility selectivity for the separation of target HFCs mixtures. Based on the available vapor–liquid equilibrium (VLE) data, a recent review presented the UC-RAIL database, a compendium of data that comprehensively assessed the performance of 52 ILs to separate refrigerant blends [1]. The quest for the most suitable ILs to separate blends of fluorinated gases is also being pursued from quantum chemistry [19–21] and molecular dynamics [22–25] approaches.

^{*} Corresponding authors.

E-mail addresses: zarzag@unican.es (G. Zarca), urtiaga@unican.es (A. Urtiaga).

<https://doi.org/10.1016/j.seppur.2023.124610>

Received 13 February 2023; Received in revised form 7 July 2023; Accepted 16 July 2023

Available online 20 July 2023

1383-5866/© 2023 The Author(s). Published by Elsevier B.V. This is an open access article under the CC BY-NC-ND license (<http://creativecommons.org/licenses/by-nc-nd/4.0/>).

The design of ED processes using ILs to separate refrigerant blends is a field of research of growing interest in which the pioneering work of Shiflett and Yokozeki [26] is remarkable in reporting the separation of the components of the R-410A mixture by an ED process using 1-butyl-3-methylimidazolium hexafluorophosphate, $[\text{C}_4\text{C}_1\text{im}][\text{PF}_6]$. More recent works have improved the separation process layout with the aim to increase the product purity above 99.5 wt% so as to comply with the purity constraints for recycled refrigerants imposed by the AHRI Standard 700. In particular, Finberg and Shiflett [27] conducted the process optimization through sensitivity analyses performed to different process variables (namely, solvent-to-feed ratio, pressure, reflux ratio, and feed stage) to reach a product purity of 99.56 wt%. Initially, this procedure was executed also with 1-ethyl-3-methylimidazolium bis(trifluoromethylsulfonyl)imide ($[\text{C}_2\text{C}_1\text{im}][\text{TF}_2\text{N}]$) as entrainer, yet only $[\text{C}_4\text{C}_1\text{im}][\text{PF}_6]$ achieved the product quality requirements due to the very low selectivity offered by $[\text{C}_2\text{C}_1\text{im}][\text{TF}_2\text{N}]$. Finally, Monjur et al. [28] went a step further and developed an ED process synthesis framework, using $[\text{C}_4\text{C}_1\text{im}][\text{PF}_6]$, that was rigorously optimized for the minimum equivalent work consumption and separation cost. As can be seen, these valuable works are mostly focused on the use of $[\text{C}_4\text{C}_1\text{im}][\text{PF}_6]$, a rather viscous IL (~ 400 mPa·s at 293.15 K) that may hinder achieving the degree of separation expected from the results obtained with equilibrium-based ED designs, except at high operating temperatures. In fact, the previous designs operated the reboiler at relatively high temperatures (above 370 K), but this was required to increase the product purity as consequence of the low solubility selectivity of $[\text{C}_4\text{C}_1\text{im}][\text{PF}_6]$.

Moreover, the abovementioned works reported the design and optimization of ED processes under equilibrium conditions that will most likely not be satisfied when using ILs as entrainers because of the high viscosity of most ILs, and the effect of such property on reducing mass transfer kinetics [29,30]. Rather than assuming that the gas and liquid phases are in equilibrium in the whole system (equilibrium model), the non-equilibrium or rate-based models consider the gases to be in equilibrium only at the gas–liquid interface. Thus, the gas concentrations in the bulk of the liquid phase are determined by the diffusion rate (kinetic regime), which enables to describe the column concentration profiles more precisely than the equilibrium model [31–34]. This approach has been previously assessed for other azeotropic mixtures, but not to a large extent [35], for instance, Meindersma et al. [36] and Quijana-Maldonado et al. [37,38] studied the effect of mass transfer kinetics on the design of ILs-based ED processes for separating ethanol/water mixtures, and highlighted the relevance of the IL viscosity on the separation performance and energy consumption. Liu et al. [39] studied the separation of dimethyl carbonate/methanol, and revealed that the liquid film offered a relevant mass transfer resistance, which was also influenced by the packing structure.

In this work, we hypothesized that a rational selection of ILs together with a rate-based analysis of the separation process are essential to improve the process design and achieve more realistic results. Therefore, this work explores the ED separation of R-410A, an equimass mixture of R-32 and pentafluoroethane (R-125), for which the VLE presents very low temperature glide. There is a growing interest in the recovery of R-32, as this refrigerant is being used as replacement of R-410A, as well as in the formulation of alternative, low-GWP HFC/HFO blends, such as R-454C, R-459B, and R-457A [40–42]. First, a selection of ILs based on their structure–property relationships was conducted considering those ILs for which the VLE of R-32 and R-125 had been experimentally described over a wide range of pressures and temperatures. For the selected ILs, the VLE data were accurately described with the Non-Random Two-Liquid (NRTL) thermodynamic model, and the ED process was designed using equilibrium and rate-based models to evaluate the relevance of considering mass transfer limitations in the IL phase. To that end, three ILs with different absorption, selectivity and viscosity properties were eventually selected and analyzed: (i) 1-butyl-3-methylimidazolium hexafluorophosphate ($[\text{C}_4\text{C}_1\text{im}][\text{PF}_6]$), (ii) 1-ethyl-methylimidazolium thiocyanate ($[\text{C}_2\text{C}_1\text{im}][\text{SCN}]$), and (iii) 1-hexyl-3-

methylimidazolium bis(trifluoromethylsulfonyl)imide ($[\text{C}_6\text{C}_1\text{im}][\text{TF}_2\text{N}]$). Among them, various operating and design variables, namely the required number of stages, the solvent-to-feed ratio, the reflux ratio, the feed stage and the height equivalent to a theoretical plate (HETP) parameter, were fine-tuned to minimize the overall energy consumption, with the final goal of determining which IL entrainer was more appropriate for recovering both R-32 and R-125 with a minimum purity of 99.5 wt% each. Overall, this work provides insights on the benefits of using low viscosity ILs with elevated solubility selectivity, in contrast to previous studies in which the elevated absorption capacity was the preferred IL property. In this way, this paper contributes to the global goal of climate change mitigation by bringing forward meaningful advances for the reclamation of fluorinated hydrocarbons.

2. Ionic liquid screening

The entrainer is the core element in the design of an ED process [35,43]. It is essential to have an accurate knowledge of the system phase behavior, which must be adequately described by thermodynamic models that will be incorporated to the simulation of the ED separation process. For this, the NRTL activity coefficient model was chosen given its accuracy to describe the VLE of F-gas/IL systems [1] and its widespread implementation in Aspen Plus process simulator [33,37,44]. Table S1 (Supporting Information) collects the initial group of 37 IL candidates, of which more than 20 ILs present VLE data of absorption of R-32 and R-125 [1,45,46]. The contents of Table S1 include the number of VLE datapoints available in literature for each pair IL/R-32 and IL/R-125. Other columns inform about the range of temperatures and pressures in which the VLE was characterized, the IL viscosity and its melting point. Next, we selected the ILs for which there are VLE data over a wide range of temperatures and pressures, which will enable to perform a trustworthy thermodynamic adjustment [47]. Also, ILs that exhibited viscosity above 100 mPa·s at 318.15 K and/or a melting point higher than 288.15 K were discarded. Thus, seven imidazolium-based ILs, with two, four, and six-carbon alkyl chains in the cation, and different anion moieties ($[\text{PF}_6]^-$, $[\text{TF}_2\text{N}]^-$, $[\text{BF}_4]^-$, $[\text{dca}]^-$, and $[\text{SCN}]^-$) were selected, including non-fluorinated ILs that exhibit higher solubility selectivity at the expense of relatively lower absorption capacity.

After this first screening, deeper insight into the desired properties of potential IL candidates was gained by considering three relevant factors: 1) the absorption capacity of the IL towards R-32 (AC_{R-32}); 2) the separation factor of the components of the R-410A binary mixture (α_{R-410A}), calculated at 318.15 K and 1.4 MPa, conditions selected from previous literature [27]; and 3) the IL viscosity at the same temperature and atmospheric pressure [48–53]. Both AC_{R-32} and α_{R-410A} have a significant impact on ED variables such as the packed column height, the solvent-to-feed ratio (S/F), and the column temperature profile, which will have an impact on the energy requirements and the economics [54,55]. AC_{R-32} and α_{R-410A} were determined from non-competitive VLE data according to Equations (1) and (2) [13]:

$$AC_{R-32} = \frac{x_{R-32}}{(1 - x_{R-32}) \cdot MW_{IL}} \quad (1)$$

$$\alpha_{R-410A} = \frac{y_{R-125}/x_{R-125}}{y_{R-32}/x_{R-32}} \quad (2)$$

where MW_{IL} is the molecular weight of the IL, and x and y are the molar fraction of the refrigerant gases in the liquid and gas phases, at 318.15 K and 1.4 MPa.

Fig. 1 presents the seven ILs ordered from the highest to the lowest viscosity at 318.15 K, where $[\text{C}_4\text{C}_1\text{im}][\text{PF}_6]$ is the most viscous IL (94 mPa·s) and $[\text{C}_2\text{C}_1\text{im}][\text{dca}]$ the least (9 mPa·s). Based on this overall view, three ILs with opposite properties were selected to evaluate their performance in the design of the non-equilibrium ED process to recover R-32 from R-410A. On the one hand, $[\text{C}_4\text{C}_1\text{im}][\text{PF}_6]$ was selected because it has the highest AC_{R-32} (4.25 mol R-32/kg IL), but exhibits a

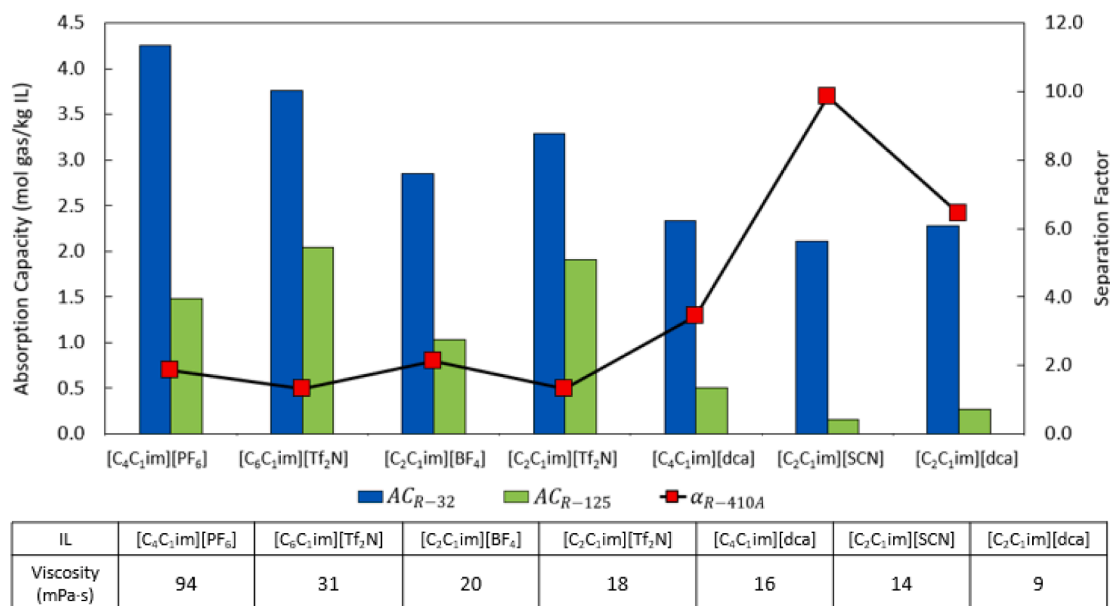


Fig. 1. R-32 and R-125 absorption capacity, and R-410A separation factor of seven ILs at 318.15 K and 1.4 MPa, as well as IL viscosity at 318.15 K and atmospheric pressure.

relatively low α_{R-410A} (1.85). In addition, this IL allowed to validate our methodology with previous works [27,28]. Secondly, $[C_2C_1im][SCN]$ was selected as it presents the highest α_{R-410A} (9.85) and a very low viscosity (14 mPa·s), although at the cost of a lower AC_{R-32} (2.11 mol R-32/kg IL). Lastly, $[C_6C_1im][Tf_2N]$ was chosen as an IL with moderate viscosity (31 mPa·s), and high absorption capacity of both R-32 and R-125 and thus, a very low α_{R-410A} (1.31).

3. Separation process design

3.1. Design basis

The ED process consists of the three units shown in Fig. 2: (i) the extractive distillation column (EDC), (ii) the recovery of the entrainer in two flash evaporators placed in series, and (iii) the solvent reconditioning before being recirculated to the EDC. Firstly, the blend R-410A (50 wt% R-32 and 50 wt% R-125) and the IL entrainer are fed to the EDC, a packed column, where the IL preferentially absorbs R-32. Thereby, R-125 becomes the distillate stream, and the IL with the absorbed R-32 the bottoms stream. Different alternative configurations can be applied to recover the IL [16,28], such as another distillation column [56,57], a flash unit [19,27], or two flash units in series [26,58]. Monjur et al. [28] concluded that the use of two flash units in series (F1,

F2) is the best option in terms of sustainability and economics. Finally, the pressure and temperature of the IL are adjusted before returning it to the EDC using a pump and a heat exchanger.

In this work, we used the process simulator Aspen Plus v11 to design the ED process. The RadFrac block was selected to simulate the EDC operation, as it supports the definition of the model to be adopted, either equilibrium or rate-based. In addition, it provides a set of different types of packing and correlations to describe the kinetic behavior of the phases. Among those available, the Mellapak 750Y Sulzer-structured packing was selected, as it is widely employed due to its high surface area [36,59]. The correlations of Bravo et al. [60] to describe the mass transfer and the method of Chilton and Colburn [61] for the heat transfer were used in this work. In this selection, we followed the recommendations of Quijada-Maldonado et al. [37], who validated the accuracy of the simulation of the IL-based water/ethanol ED process with pilot-plant experimental data.

In addition, the following heuristics were considered to design the ED process. The feed flowrate of R-410A (100 kg/h) was introduced as a liquefied stream at the operating pressure, which enhances the separation performance with respect to introducing the feed in vapor phase [27], and the IL stream was fed at 288.15 K. The EDC was operated at 1.4 MPa for $[C_4C_1im][PF_6]$ and $[C_6C_1im][Tf_2N]$, and 1.0 MPa for $[C_2C_1im][SCN]$ because this IL exhibits much higher selectivity and therefore, it is possible to operate the EDC at lower temperature and consequently, at lower pressure to avoid liquefaction of the HFCs within the EDC. On the quest for a total R-32/R-125 separation, the distillate rate was fixed at 50 kg/h. Moreover, as ILs have negligible vapor pressure, the IL feed stage was set at the top of the column to ensure the maximum contact between gas and liquid streams [62–64]. Regarding the flash operation, the temperature was set equal to the reboiler temperature to reduce the energy requirements, and the first flash drum was operated at atmospheric pressure, while the pressure in the second one was set at 0.01 MPa, following previous works that proved the viability of this scheme to regenerate the IL [26,28,58].

To acquire reliable results in the equilibrium and rate-based process simulations, the physical and transport properties of the ILs must be defined. Tables S2-S6 of the Supporting Information (SI) collect all the required properties of the selected ILs (normal boiling point, critical temperature, pressure and molar volume, compressibility factor, acentric factor, and the Rackett's compressibility factor) as well as the

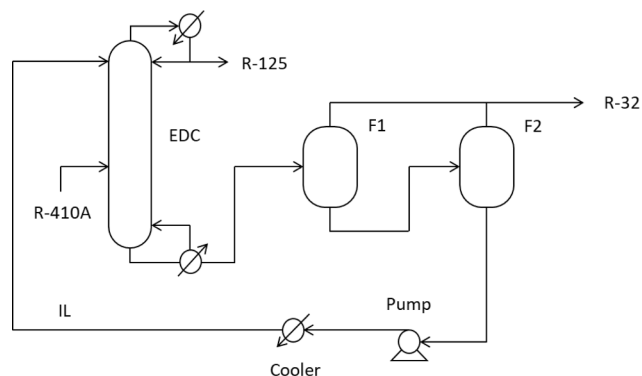


Fig. 2. ED separation process flow diagram including the IL regeneration and conditioning steps.

models used to describe the temperature-dependent properties: ideal gas and liquid heat capacities, vapor pressure, heat of vaporization, viscosity, and surface tension. In addition, Table S7 includes the NRTL parameters of the ILs.

3.2. Design procedure

The design procedure consisted of a sequential (hierarchical) workflow in which the first step was the calculation of the EDC considering the equilibrium model. Fig. 3A shows the workflow followed in this first step to fine-tune the number of theoretical stages, the R-410A inlet stage, the S/F ratio, and the reflux ratio, aiming to conceive the design with the minimum number of stages that satisfies the required purity of 99.5 wt% R-32 at the exit of the flash units. At this point, some maximum limits were considered: a reflux ratio value of 4, S/F ratio of 20, and maximum number of theoretical stages of 40, including condenser and reboiler [27,28,56].

Next, the ED process design based on the rate-based model was implemented (Fig. 3B) starting from the result of the equilibrium-based design (result of Fig. 3A), and finally, the stepwise rate-based design was performed, as described in Fig. 3C. The rate-based model was initialized with an HETP parameter of 0.17 m, as specified by the packing manufacturer [38,65]. For the optimization of the ED rate-based design, in case the required product purity was not achieved after shifting from the equilibrium to the non-equilibrium model, first the packing height was increased by adjusting the HETP to obtain an initial rate-based design that satisfies the purity requirements. Then, the operation variables (feed stage, S/F ratio and HETP) were adjusted by sensitivity analyses to minimize the energy consumption and avoid flooding phenomena, which would lead to a significant increase in pressure drop, liquid hold-up and loss in separation efficiency [66]. Finally, the economic evaluation of the best process design for each IL was undertaken following the cost estimation methodology described in the SI.

4. Results and discussion

4.1. Equilibrium vs. Rate-based ED process design

This section analyzes the relevance of applying a rate-based model in the design of the ED process for the separation of R-410A when using ILs as entrainers. For this purpose, the ED column was first designed with the equilibrium model to reach the 99.5 wt% purity products, following the method described in Fig. 3A. The ED process layout using $[C_2C_1im][SCN]$ as entrainer is shown in Fig. 4, which illustrates the main process and equipment variables (in black and blue colors). Throughout the rest of this article, the figures present the $[C_2C_1im][SCN]$ results because this is the most interesting IL for the R-410A separation among those evaluated. Once obtained these equilibrium model-based designs, the model was changed to the non-equilibrium to recalculate the purity of the product streams considering the rate of mass transfer under the same process design. As a consequence, the compositions of the distillate and bottoms streams and exiting streams from the flash units were altered (results written in orange color in Fig. 4). The analogous process flow diagrams that result from using $[C_4C_1im][PF_6]$ and $[C_6C_1im][Tf_2N]$ as entrainers are presented in Figures S1 and S2 of the SI.

As can be seen, in the case of considering the equilibrium model, an 18-stage column (excluding condenser and reboiler), a S/F ratio of 5.80 and a reflux ratio of 1.4 were required with the IL $[C_2C_1im][SCN]$ to reach the target product purity (99.55 wt% R-125 in the distillate and 99.55 wt% R-32 in the outlet stream of the second flash unit, respectively). However, the products purity decreased to 94.09 wt% if the rate-based model is considered for the same column and operating conditions. Similar results were obtained with the IL $[C_4C_1im][PF_6]$ (Figure S1 in the SI), yet at the expense of increasing the S/F ratio to 6.75, a similar design to that presented by Finberg & Shiflett [27]. However, considering $[C_6C_1im][Tf_2N]$, an IL with low solubility selectivity for this separation, very significant differences in the product purity were observed between the results of equilibrium and rate-based

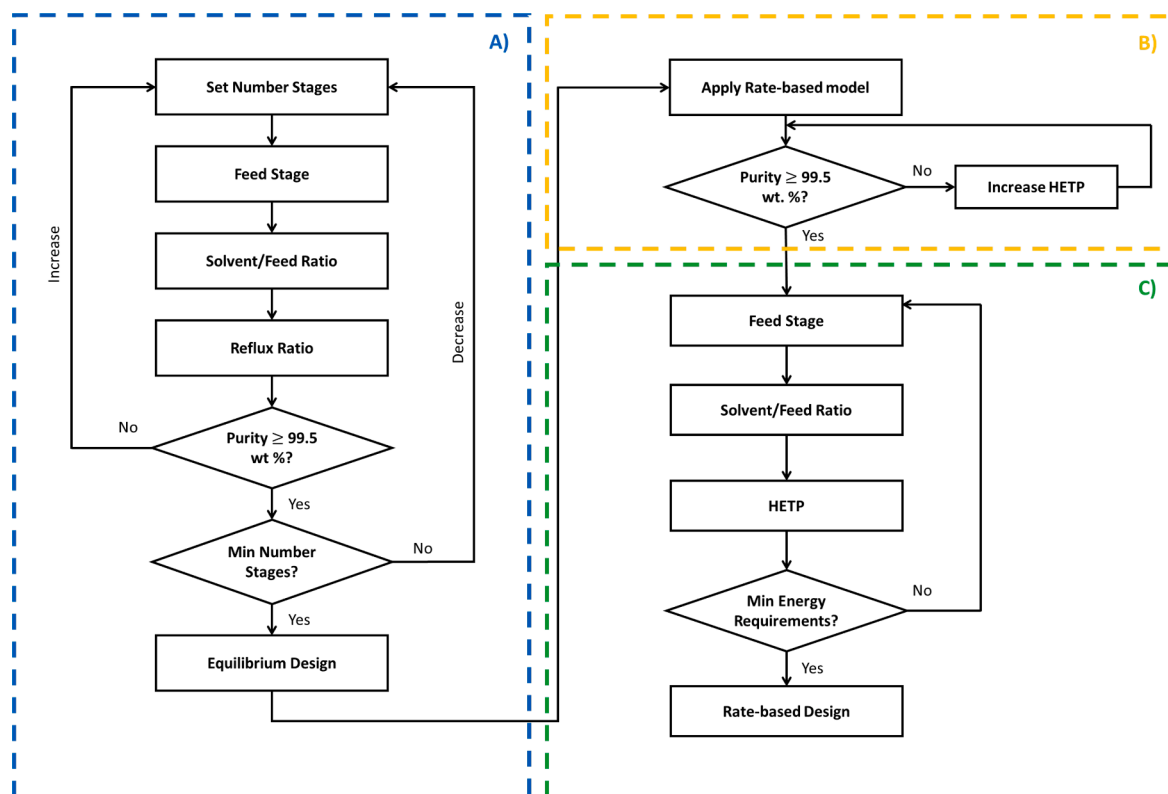


Fig. 3. Design workflow: A) Equilibrium design, B) Rate-based initialization, and C) Rate-based design.

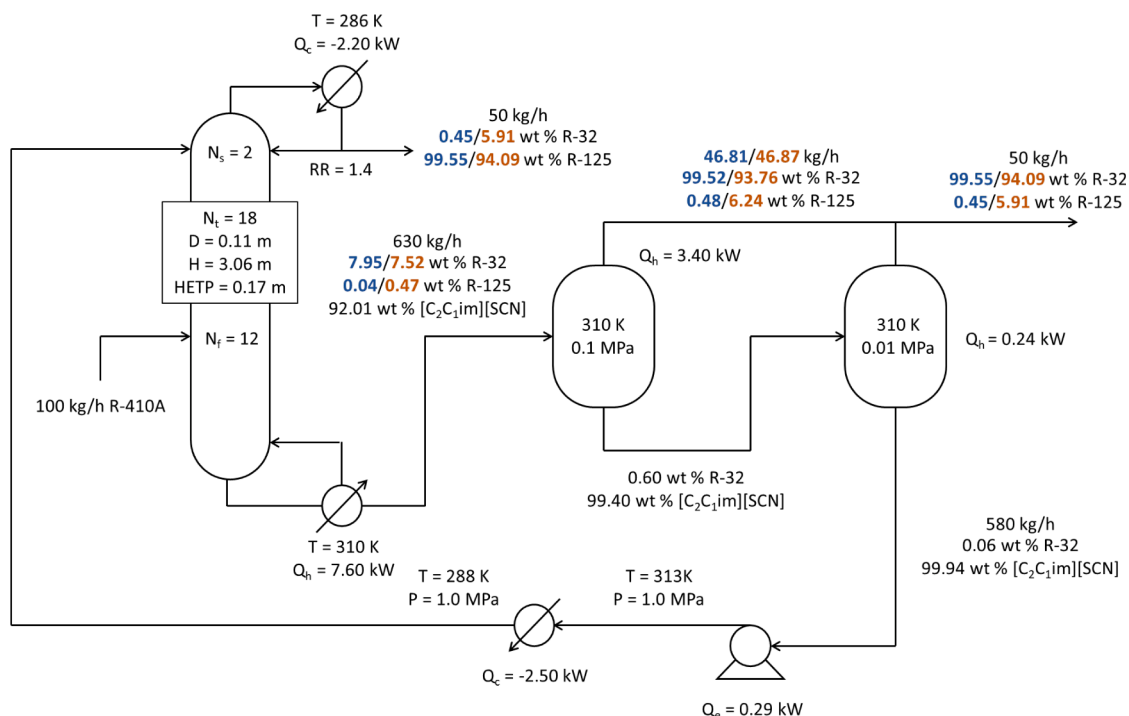


Fig. 4. ED process flow diagram of R-410A separation, using $[C_2C_1im][SCN]$ as entrainer, derived from the equilibrium step (blue). The results in orange correspond to the same process design (equal number of stages, reflux ratio and S/F ratio), but shifting the model to rate-based, that is, the non-optimal rate-based design (orange).

models (Figure S2 of the SI). Under equilibrium considerations, the maximum product purity achieved was 95.12 wt% with the maximum S/F ratio and number of stages defined in Section 3.2 (reflux ratio of 4, S/F ratio of 20), which would lead to discard this IL as entrainer in a preliminary assessment due to its low solubility selectivity. In contrast, the performance of $[C_6C_1im][Tf_2N]$ was greatly improved when the rate-based model was applied, although the target purity was not achieved either. These differences are a consequence of the evaluation of the gas diffusion rate in the EDC and the fact that, when the equilibrium model is applied, the concentration of R-32 and R-125 reaching the bulk of the IL is overestimated. Therefore, it becomes clear that mass transfer plays a key role in the performance of EDCs with IL entrainers and consequently, the rate-based model should be considered in the

separation process design.

4.2. Influence of IL properties on the rate-based process design

Prior to the rate-based design and following the procedure described in Fig. 3B, the HETP parameter was initially increased from the equilibrium design value (0.17 m) until obtaining initial rate-based designs in which the target purity of 99.5 wt% was reached for the three ILs. This is achieved with 0.22 m for $[C_4C_1im][PF_6]$ and $[C_6C_1im][Tf_2N]$, and 0.45 m for $[C_2C_1im][SCN]$. Next, the stepwise design of the rate-based ED process was performed assessing the influence of the feed stage position, the S/F ratio and the HETP parameter on the purity of products. The feed stage defines the extraction section of the column, directly

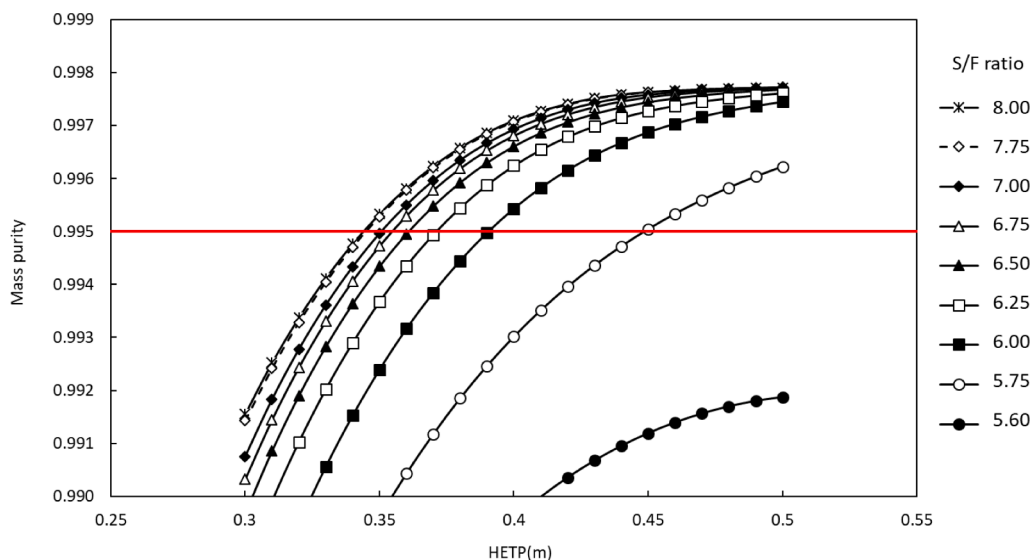


Fig. 5. Purity of products as a function of the HETP and S/F ratio using $[C_2C_1im][SCN]$ as entrainer. The red line represents the target product purity.

influencing the products purity. The influence of this variable is described in Section 5 of the SI, showing a similar trend when the equilibrium or rate-based model was used for the three ILs.

Fig. 5 shows the influence of the S/F ratio and of the HETP parameter, on the products quality when the ED column was furnished with $[C_2C_1im][SCN]$. As can be seen, for S/F ratios lower than 5.75 the product purity specification is not achieved for any HETP value. Moreover, for a fixed R-410A feed flowrate, increasing the IL flowrate or the packing height led to higher product purity up to an asymptotic value of 99.8 wt%. For the case of $[C_2C_1im][SCN]$, the minimum HETP that satisfied the target purity was 0.33 m coupled with a $S/F = 7.75$ (IL flowrate of 775 kg/h). A further increase of the entrainer flowrate did not provide a noticeable improvement on the products purity, as can be seen when a S/F ratio of 8.0 was applied. Moreover, reducing the IL flowrate was only possible at the expense of increasing the HETP. Consequently, numerous points that meet the target purity can be identified in Fig. 5. The analysis of the other two IL entrainers, $[C_4C_1im][PF_6]$ and $[C_6C_1im][Tf_2N]$, was also performed showing similar trends to that found for $[C_2C_1im][SCN]$, although with significant differences in the magnitude of the S/F values obtained (Figures S4 and S5 of the SI).

To gain deeper insight into the best ED process design for each IL, the energy consumption was thoroughly analyzed. The total energy required (TER) to separate one kg of the refrigerant blend R-410A into their components R-32 and R-125 with 99.5 wt% purity was calculated as the absolute sum of the energy requirements of each process unit, considering the following contributions: (i) the heat used in the reboiler and flash units (Q_h), (ii) the cooling demands of the condenser and cooler (Q_c), and (iii) the electricity (W) consumed by the pump to pressurize the IL. For $[C_2C_1im][SCN]$, the energy demands of the different process units are summarized in Fig. 6 for the scenarios selected, which included the two extreme points, that is, the one with the lowest IL flowrate and highest HETP ($S/F = 5.75$, HETP = 0.45 m), and the one with the lowest HETP and the highest flowrate ($S/F = 7.75$, HETP = 0.33 m), plus two intermediate cases ($S/F = 6.0$, HETP = 0.39 m; and $S/F = 6.5$, HETP = 0.36 m). The conditions used for the analysis of the analogous scenarios for the other ILs are collected in Table S10 of the SI.

In all cases, the reboiler was the most energy intensive equipment, followed by flash 1 and the cooler. The energy of the second flash and the pump accounted for less than 3% of the total energy demands, in the worst case. By analyzing the effect of the IL flowrate, the process units could be divided in three groups. The first one gathers the reboiler, the cooler and the pump, whose energy requirements increased on increasing the IL flowrate and reboiler temperature, because more en-

ergy is needed to desorb the gas in the reboiler and to reduce the temperature of the IL before entering the ED column. For the second group, composed of the flash drums, increasing the IL flowrate posed a positive effect because the gas expansion lowered the cooling requirements. Lastly, the condenser is not influenced by the IL flowrate, and its energy demand remained constant in all the cases analyzed. All considered, there is a direct relationship between the S/F ratio and reboiler temperature with the TER of the process, which ranged between 0.168 and 0.213 kWh/kg R-410A treated with $[C_2C_1im][SCN]$ as the IL entrainer.

The same analysis was conducted with the other two IL entrainers, $[C_4C_1im][PF_6]$ and $[C_6C_1im][Tf_2N]$, obtaining analogous trends that are described in Figures S6 and S7 of the SI. A summary of the optimal ED process designs for each IL is collected in Table 1, and the analysis of the equipment contributions to the global energy consumption and the economic analysis are depicted in Fig. 7. The IL $[C_2C_1im][SCN]$ led to the lowest TER, 0.168 kWh/kg R-410A, which is 28% lower than that achieved with $[C_4C_1im][PF_6]$, and about one-seventh compared to using $[C_6C_1im][Tf_2N]$. The main differences were observed in the requirements of the reboiler and the cooler, which increased greatly in the order $[C_2C_1im][SCN] < [C_4C_1im][PF_6] < [C_6C_1im][Tf_2N]$. Regarding the process economics, a similar trend was observed. The lowest unitary cost (UC), i.e. the cost of treating one kg of R-410A, is attained with the $[C_2C_1im][SCN]$ -based design, 0.044 \$/kg R-410A, which is 10% and 66% lower than for $[C_4C_1im][PF_6]$ and $[C_6C_1im][Tf_2N]$, respectively. This is mainly attributed to the IL solubility selectivity, that is, a lower separation factor implies the need of a higher EDC temperature profile. This leads to more energy being required in the reboiler and the cooler, and consequently to higher operating costs, since the latter has to chill a larger amount of entrainer that exits the EDC at a higher temperature. In particular, the energy requirements in both units (reboiler and cooler)

Table 1

Characteristics of the best rate-based ED process designs according to the energy consumption analysis. $F = 100$ kg/h R-410A.

IL	Reboiler Temperature (K)	S/F Ratio	Packing Height (m)	Total Energy Requirements (kWh/kg R-410A)	Unitary Costs (\$/kg R-410A)
$[C_2C_1im][SCN]$	310	5.75	8.10	0.168	0.044
$[C_4C_1im][PF_6]$	333	4.0	7.56	0.234	0.051
$[C_6C_1im][Tf_2N]$	382	14.5	13.49	1.122	0.136

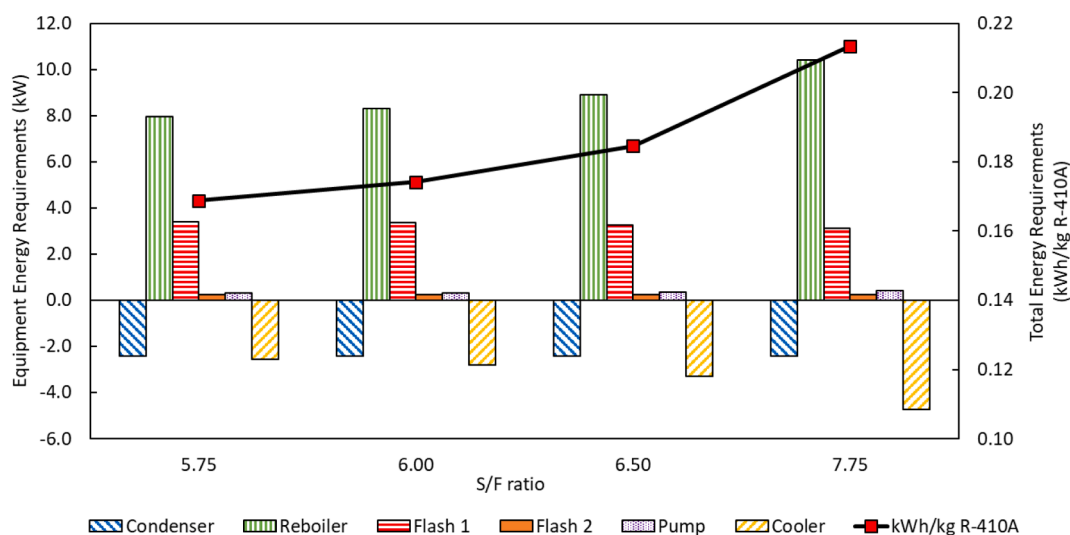


Fig. 6. Energy requirements of rate-based ED process designs with $[C_2C_1im][SCN]$.

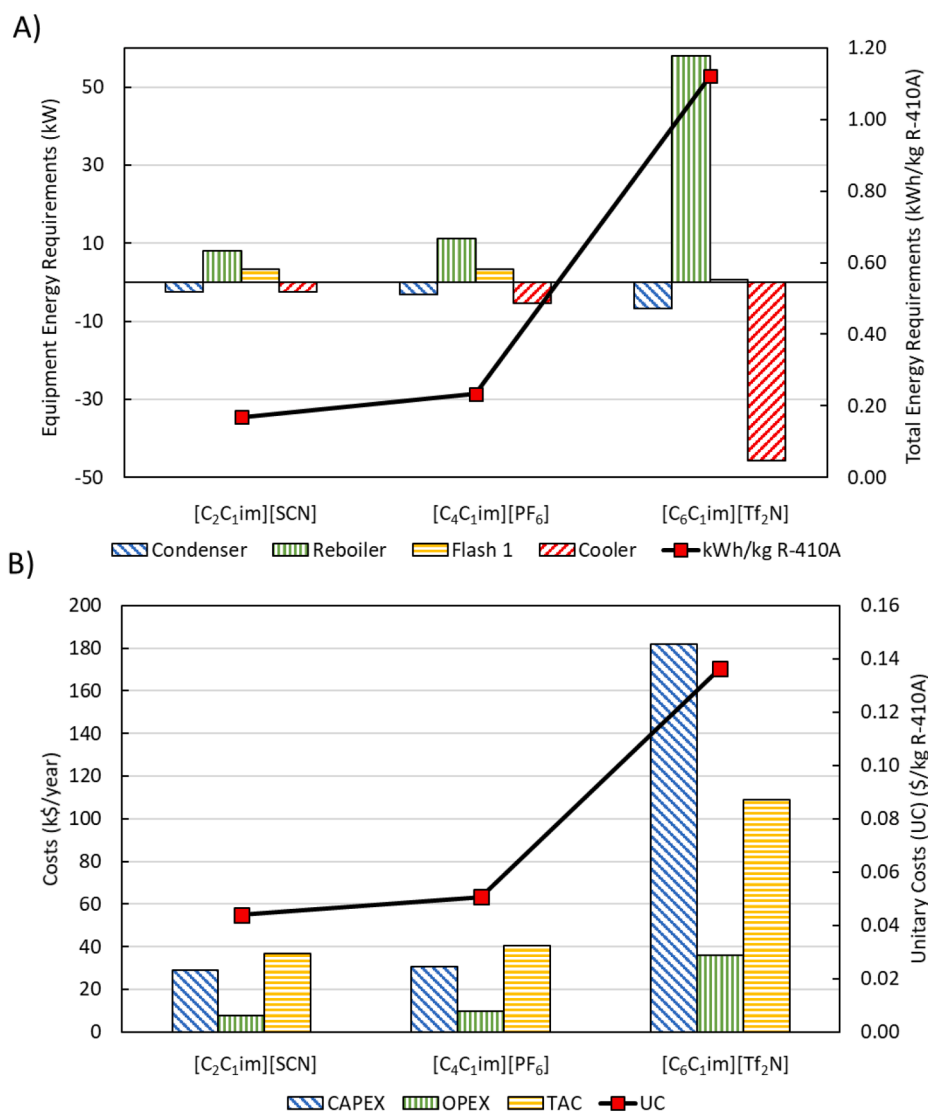


Fig. 7. Comparison of the energy requirements (A) and the process economics (B) among the lowest energy consumption designs of the three ILs [C₂C₁im][SCN], [C₄C₁im][PF₆] and [C₆C₁im][Tf₂N].

were one order of magnitude higher in the [C₆C₁im][Tf₂N]-based design than for the other two ILs. This was also true for the condenser and the pump, but to a lesser extent. Regarding the flash units, the opposite trend was observed, as the cooling effect produced by the gas desorption decreased when the volume of solvent was increased, which entailed less energy to be applied for the isothermal flash operation. Another disadvantage of using a higher *S/F* ratio is the requirement of larger equipment sizes, resulting in higher costs, as observed in the design of the the [C₆C₁im][Tf₂N] with respect to those of [C₂C₁im][SCN] and [C₄C₁im][PF₆] in Fig. 7B.

Therefore, in view of the energy and economics results, the separation factor α_{R-410A} is placed as one of the key properties to evaluate for selecting the IL entrainer, as its influence on the rate-based ED process design is more significant than the IL absorption capacity *AC*. Particularly, in the search of the best IL entrainer for the separation of the R-410A refrigerant mixture, the high R-32 sorbing but low selective [C₆C₁im][Tf₂N] was discarded (Figure S15). Comparing the separation process designs between the highly selective [C₂C₁im][SCN] with low R-32 absorption capacity (Fig. 8), and the high R-32 sorbing [C₄C₁im][PF₆] with low solubility selectivity (Figure S11), the use of [C₂C₁im][SCN] demands 28% less energy to achieve 99.5 wt% purity of the gas products, which leads to similar investment costs but 20% lower

operation costs in comparison with [C₄C₁im][PF₆]. Thus, this work points to the non-fluorinated [C₂C₁im][SCN] as an excellent IL entrainer for separating the R-410A refrigerant mixture with the minimum TER and UC.

5. Conclusions

In this work, the influence of IL entrainer properties on the design of ED processes to separate the close boiling R-410A refrigerant blend into its main components, R-32 and R-125, is reported considering mass transfer phenomena (rate-based model), and the results compared to those obtained with an equilibrium model. Given the higher viscosity of ILs compared to conventional solvents, the need to consider mass transfer phenomena in the design of the separation process was reflected.

Regarding the selection of the most suitable solvent, the influence of IL properties such as the absorption capacity and the separation factor were evaluated. The latter was found to be the most influential parameter in the design of the ED process with rate-based models, as a higher α leads to lower energy and economic requirements. This rational assessment of ILs together with a rate-based analysis of the separation process led us to select the non-fluorinated IL [C₂C₁im][SCN] as one of

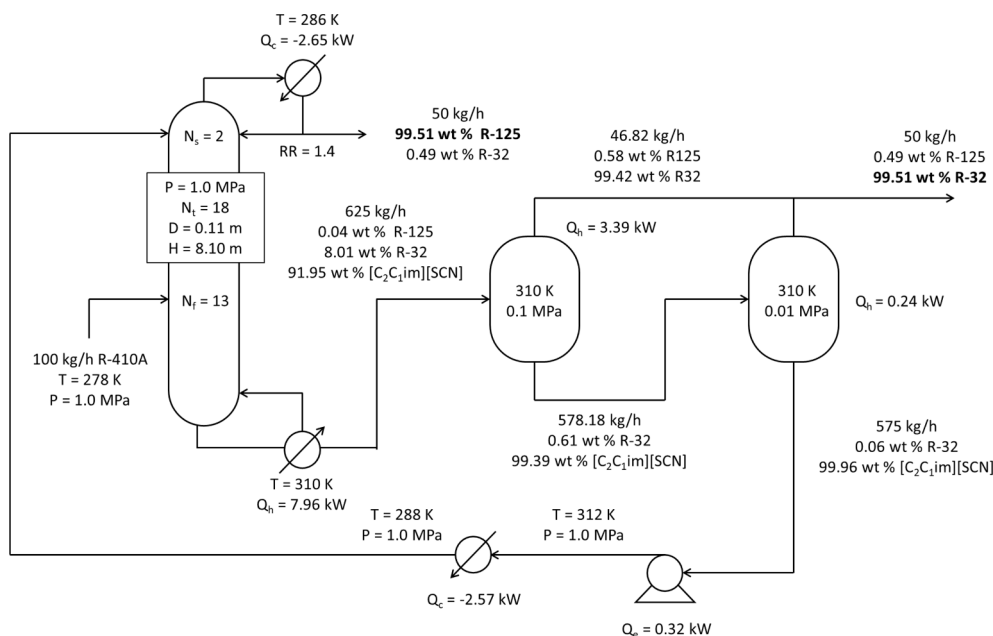


Fig. 8. Rate-based ED process flow diagram with the lowest TER requirements (0.168 kWh/kg R-410A) and UC (0.044 \$/kg R-410A).

the most promising ILs for the separation of R-410A because of its attractive α_{R-410A} (9.85) and very low viscosity, ahead of ILs with higher absorption capacity proposed in previous works.

More specifically, $[C_2C_1im][SCN]$ allows the separation of the target R-410A blend into its components R-32 and R-125 with a purity of 99.5 wt% using an 8.1 m height column, a S/F ratio of 5.75 and a low temperature profile (286–310 K), which can be translated into a consumption of 0.168 kWh/kg R-410A and an estimated cost of 0.044 \$/kg R-410A. Moreover, we expect that the resulting ED design with $[C_2C_1im][SCN]$ can be further improved following a rigorous optimization procedure, analogous to that performed by Monjur et al. [28] for $[C_4C_1im][PF_6]$, but considering rate-based models.

In view of the results obtained, further development of IL-based ED processes to separate refrigerant mixtures should consider the rate-based model and prioritize the search of ILs with high selectivity and low viscosity, instead of ILs with high sorption capacity, if it is expected that the equilibrium conditions are not attained within the ED column. In addition, experimental data on mixture viscosity for the systems of greatest interest are required to account for excess viscosity effects on the process design. Overall, this work contributes to the design of enabling technologies for the selective separation of refrigerants, which is essential to minimize the uncontrolled emissions of high-GWP hydrofluorocarbons and boost the recovery and recycling of these value-added compounds.

CRediT authorship contribution statement

Miguel Viar: Investigation, Software, Formal analysis, Writing – original draft, Data curation. **Salvador Asensio-Delgado:** Investigation, Software, Methodology. **Fernando Pardo:** Investigation, Formal analysis, Supervision, Data curation. **Gabriel Zarca:** Conceptualization, Methodology, Writing – review & editing, Supervision. **Ane Urriaga:** Conceptualization, Methodology, Funding acquisition, Writing – review & editing, Supervision, Project administration.

Declaration of Competing Interest

The authors declare that they have no known competing financial interests or personal relationships that could have appeared to influence the work reported in this paper.

Data availability

Data will be made available on request.

Acknowledgements

The authors acknowledge the financial support of MCIN/AEI/10.13039/501100011033 and the European Union NextGenerationEU/PRTR to projects PID2019-105827RB-I00 and TED2021-129844B-I00. F. Pardo thanks the postdoctoral fellowship IJC2020-043134-I “Juan de la Cierva Incorporación”. M. Viar thanks the Concepcion Arenal UC-22-23 pre-doctoral fellowship, funded by the University of Cantabria and the Government of Cantabria.

Appendix A. Supplementary material

Supplementary data to this article can be found online at <https://doi.org/10.1016/j.seppur.2023.124610>.

References

- [1] S. Asensio-Delgado, F. Pardo, G. Zarca, A. Urriaga, Absorption separation of fluorinated refrigerant gases with ionic liquids: Equilibrium, mass transport, and process design, *Sep. Purif. Technol.* 276 (2021), 119363, <https://doi.org/10.1016/j.seppur.2021.119363>.
- [2] S. Asensio-Delgado, F. Pardo, G. Zarca, A. Urriaga, Enhanced absorption separation of hydrofluorocarbon/hydrofluoroolefin refrigerant blends using ionic liquids, *Sep. Purif. Technol.* 249 (2020), 117136, <https://doi.org/10.1016/j.seppur.2020.117136>.
- [3] A.D. Yancey, D.R. Corbin, M.B. Shiflett, Difluoromethane (HFC-32) and pentafluoroethane (HFC-125) sorption on linde type A (LTA) zeolites for the separation of azeotropic hydrofluorocarbon refrigerant mixtures, *Langmuir* 38 (2022) 1937–1953, <https://doi.org/10.1021/acs.langmuir.1C02904>.
- [4] M.M. El-Sharkawy, A.A. Askalany, K. Harby, M.S. Ahmed, Adsorption isotherms and kinetics of a mixture of pentafluoroethane, 1,1,1,2-tetrafluoroethane and difluoromethane (HFC-407C) onto granular activated carbon, *Appl. Therm. Eng.* 93 (2016) 988–994, <https://doi.org/10.1016/j.applthermaleng.2015.10.077>.
- [5] A.B. Pereiro, J.E. Sosa, R.P.P.L. Ribeiro, P.J. Castro, J.P.B. Mota, J.M.M. Araújo, Sorption of fluorinated greenhouse gases in silica-supported fluorinated ionic liquids, *J. Environ. Chem. Eng.* 10 (2022), 108580, <https://doi.org/10.2139/ssrn.4130037>.
- [6] R.P. Ribeiro, J.E. Sosa, J.M. Araújo, A.B. Pereiro, J.P. Mota, Vacuum swing adsorption for R-32 recovery from R-410A refrigerant blend, *Int. J. Refrig.* (2023), <https://doi.org/10.1016/j.ijrefrig.2023.01.020>.
- [7] F. Pardo, G. Zarca, A. Urriaga, Effect of feed pressure and long-term separation performance of Pebax-ionic liquid membranes for the recovery of difluoromethane

- (R32) from refrigerant mixture R410A, *J. Memb. Sci.* 618 (2021), 118744, <https://doi.org/10.1016/j.memsci.2020.118744>.
- [8] A.N. Harders, E.R. Sturd, J.E. Vallier, D.R. Corbin, W.R. White, C.P. Junk, M. B. Shiflett, Selective separation of HFC-32 from R-410A using poly(dimethylsiloxane) and a copolymer of perfluoro(butenyl vinyl ether) and perfluoro(2,2-dimethyl-1,3-dioxole), *J. Memb. Sci.* 652 (2022), 120467, <https://doi.org/10.1016/j.memsci.2022.120467>.
- [9] F. Pardo, G. Zarca, A. Urriaga, Separation of refrigerant gas mixtures containing R32, R134a, and R1234yf through poly(ether-block-amide) membranes, *ACS Sustain. Chem. Eng.* 8 (2020) 2548–2556, <https://doi.org/10.1021/acssuschemeng.9b07195>.
- [10] F. Pardo, S.V. Gutiérrez-Hernández, P. Rodríguez-San Miguel, G. Zarca, A. Urriaga, Polymer/ionic liquid pilot scale membrane prototype for the recovery of difluoromethane (R-32) from refrigerant mixtures, *Sep. Purif. Technol.* 320 (2023), 124115, <https://doi.org/10.1016/j.seppur.2023.124115>.
- [11] M.S. Monjur, A. Iftakher, M.M.F. Hasan, Sustainable process intensification of refrigerant mixture separation and management: A multiscale material screening and process design approach, *Comput. Aided Chem. Eng.* 49 (2022) 661–666, <https://doi.org/10.1016/b978-0-323-85159-6.50110-x>.
- [12] A. Garcíadiego, M. Mazumder, B.J. Befort, A.W. Dowling, Modeling and optimization of ionic liquid enabled extractive distillation of ternary azeotropic mixtures, *Comput. Aided Chem. Eng.* 49 (2022) 307–312, <https://doi.org/10.1016/b978-0-323-85159-6.50110-x>.
- [13] S. Asensio-Delgado, M. Viar, F. Pardo, G. Zarca, A. Urriaga, Gas solubility and diffusivity of hydrofluorocarbons and hydrofluoroolefins in cyanide-based ionic liquids for the separation of refrigerant mixtures, *Fluid Phase Equilib.* 549 (2021), 113210, <https://doi.org/10.1016/j.fluid.2021.113210>.
- [14] S. Asensio-Delgado, F. Pardo, G. Zarca, A. Urriaga, Vapor-liquid equilibria and diffusion coefficients of difluoromethane, 1,1,1,2-tetrafluoroethane, and 2,3,3,3-tetrafluoropropene in low-viscosity ionic liquids, *J. Chem. Eng. Data.* 65 (2020) 4242–4251, <https://doi.org/10.1021/acs.jced.0c00224>.
- [15] A.B. Pereiro, J.M.M. Araújo, J.M.S.S. Esperança, I.M. Marrucho, L.P.N. Rebelo, Ionic liquids in separations of azeotropic systems – A review, *J. Chem. Thermodyn.* 46 (2012) 2–28, <https://doi.org/10.1016/j.jct.2011.05.026>.
- [16] Z. Lei, C. Dai, J. Zhu, B. Chen, Extractive distillation with ionic liquids: A review, *AIChE J.* 60 (2014) 3312–3329, <https://doi.org/10.1002/aic.14537>.
- [17] P.J. Castro, A.E. Redondo, J.E. Sosa, M.E. Zakrzewska, A.V.M. Nunes, J.M. M. Araújo, A.B. Pereiro, Absorption of fluorinated greenhouse gases in deep eutectic solvents, *Ind. Eng. Chem. Res.* 59 (2020) 13246–13259, <https://doi.org/10.1021/acs.iecr.0c01893>.
- [18] D. Jovell, S.B. Gómez, M.E. Zakrzewska, A.V.M. Nunes, J.M.M. Araújo, A. B. Pereiro, F. Llovel, Insight on the solubility of R134a in fluorinated ionic liquids and deep eutectic solvents, *J. Chem. Eng. Data.* 65 (2020) 4956–4969, <https://doi.org/10.1021/acs.jced.0c00588>.
- [19] H. Qin, J. Cheng, H. Yu, T. Zhou, Z. Song, Hierarchical ionic liquid screening integrating COSMO-RS and Aspen plus for selective recovery of hydrofluorocarbons and hydrofluoroolefins from a refrigerant blend, *Ind. Eng. Chem. Res.* 32 (2022) 4083–4094, <https://doi.org/10.1021/acs.iecr.1c04688>.
- [20] J.E. Sosa, R. Santiago, A.E. Redondo, J. Avila, L.F. Lepre, M.C. Gomes, J.M. M. Araújo, J. Palomar, A.B. Pereiro, Design of ionic liquids for fluorinated gas absorption: COSMO-RS selection and solubility experiments, *Environ. Sci. Technol.* 56 (2022) 5898–5909, <https://doi.org/10.1021/acs.est.2c00051>.
- [21] J.E. Sosa, R. Santiago, D. Hospital-Benito, M. Costa Gomes, J.M.M. Araújo, A. B. Pereiro, J. Palomar, Process evaluation of fluorinated ionic liquids as F-gas absorbents, *Environ. Sci. Technol.* 54 (2020) 12784–12794, <https://doi.org/10.1021/acs.est.0c05305>.
- [22] N. Wang, Y. Zhang, K.S. Al-Barghouti, R. Kore, A.M. Scurto, E.J. Maginn, Structure and dynamics of hydrofluorocarbon/ionic liquid mixtures: An experimental and molecular dynamics study, *J. Phys. Chem. B.* 2022 (2022) 8309–8321, <https://doi.org/10.1021/acs.jpcc.2c05787>.
- [23] L.F. Lepre, D. Andre, S. Denis-Quanquin, A. Gautier, A.A.H. Pádua, M. Costa Gomes, Ionic liquids can enable the recycling of fluorinated greenhouse gases, *ACS Sustain. Chem. Eng.* 7 (19) (2019) 16900–16906, <https://doi.org/10.1021/acssuschemeng.9b04214>.
- [24] S. Asensio-Delgado, F. Pardo, G. Zarca, A. Urriaga, Machine learning for predicting the solubility of high-GWP fluorinated refrigerants in ionic liquids, *J. Mol. Liq.* 367 (2022), 120472, <https://doi.org/10.1016/j.molliq.2022.120472>.
- [25] N. Wang, R.S. Defever, E.J. Maginn, Alchemical free energy and hamiltonian replica exchange molecular dynamics to compute hydrofluorocarbon isotherms in imidazolium-based ionic liquids, *J. Chem. Theory Comput.* 19 (11) (2023) 3324–3335, <https://doi.org/10.1021/acs.jctc.3c00206>.
- [26] M.B. Shiflett, A. Yokozeki, Separation of difluoromethane and pentafluoroethane by extractive distillation using ionic liquid, *Chim. Oggi - Chem. Today.* 24 (2006) 28–30.
- [27] E.A. Finberg, M.B. Shiflett, Process designs for separating R-410A, R-404A, and R-407C using extractive distillation and ionic liquid entrainers, *Ind. Eng. Chem. Res.* 60 (2021) 16054–16067, <https://doi.org/10.1021/acs.iecr.1c02891>.
- [28] M.S. Monjur, A. Iftakher, M.M.F. Hasan, Separation process synthesis for high-GWP refrigerant mixtures: Extractive distillation using ionic liquids, *Ind. Eng. Chem. Res.* 61 (2022) 4390–4406, <https://doi.org/10.1021/acs.iecr.2c00136>.
- [29] G. Zarca, A. Urriaga, I. Ortiz, P. Cañizares, M.A. Rodrigo, Carbon monoxide reactive separation with basic 1-hexyl-3-methylimidazolium chlorocuprate(I) ionic liquid: Electrochemical determination of mass transport properties, *Sep. Purif. Technol.* 141 (2015) 31–37, <https://doi.org/10.1016/j.seppur.2014.11.027>.
- [30] S. Böcker, G. Ronge, Distillation of viscous systems, *Chem. Eng. & Technol.* 28 (2005) 25–28, <https://doi.org/10.1002/ceat.200407050>.
- [31] I.V. Ivanov, V.A. Lotkhov, K.A. Moiseeva, N.N. Kulov, Mass transfer in a packed extractive distillation column, *Theor. Found. Chem. Eng.* 505 (50) (2016) 667–677, <https://doi.org/10.1134/s0040579516050304>.
- [32] J.A. Wesselingh, Non-equilibrium modelling of distillation, *Chem. Eng. Res. Des.* 75 (1997) 529–538, <https://doi.org/10.1205/026387697524083>.
- [33] M. Fontana, A.N. Marchesan, R. Maciel Filho, M.R.W. Maciel, Extractive distillation to produce anhydrous bioethanol with choline chloride with urea (1: 2) as a solvent: a comparative evaluation of the equilibrium and the rate-based models, *Chem. Eng. Process. - Process Intensif.* 168 (2021), 108580, <https://doi.org/10.1016/j.cep.2021.108580>.
- [34] Y. Song, J. Song, M. Gong, B. Cao, Y. Yang, X. Ma, Modeling of mass transfer in nonideal multicomponent mixture with Maxwell-Stefan approach, *Chinese J. Chem. Eng.* 18 (2010) 362–371, [https://doi.org/10.1016/s1004-9541\(10\)60232-7](https://doi.org/10.1016/s1004-9541(10)60232-7).
- [35] V. Gerbaud, I. Rodriguez-Donis, L. Hegely, P. Lang, F. Denes, X.Q. You, Review of extractive distillation. Process design, operation, optimization and control, *Chem. Eng. Res. Des.* 141 (2019) 229–271, <https://doi.org/10.1016/j.cherd.2018.09.020>.
- [36] G.W. Meindersma, E. Quijada-Maldonado, T.A.M. Aelmans, J.P.G. Hernandez, A. B. De Haan, Ionic liquids in extractive distillation of ethanol/water: From laboratory to Pilot plant, *ACS Symp. Ser.* 1117 (2012) 239–257, <https://doi.org/10.1021/bk-2012-1117.ch011>.
- [37] E. Quijada-Maldonado, T.A.M. Aelmans, G.W. Meindersma, A.B. de Haan, Pilot plant validation of a rate-based extractive distillation model for water–ethanol separation with the ionic liquid [emim][DCA] as solvent, *Chem. Eng. J.* 223 (2013) 287–297, <https://doi.org/10.1016/j.cej.2013.02.111>.
- [38] E. Quijada-Maldonado, G.W. Meindersma, A.B. de Haan, Ionic liquid effects on mass transfer efficiency in extractive distillation of water–ethanol mixtures, *Comput. Chem. Eng.* 71 (2014) 210–219, <https://doi.org/10.1016/j.compchemeng.2014.08.002>.
- [39] W.Z. Liu, D.S.H. Wong, S.J. Wang, H.C. Hsu, Effect of mass transfer on the design of an extractive distillation process for separating DMC and methanol, *J. Taiwan Inst. Chem. Eng.* 60 (2016) 205–212, <https://doi.org/10.1016/j.jtice.2015.11.022>.
- [40] R. Llopis, D. Calleja-Anta, D. Sánchez, L. Nebot-Andrés, J. Catalán-Gil, R. Cabello, R-454C, R-459B, R-457A and R-455A as low-GWP replacements of R-404A: Experimental evaluation and optimization, *Int. J. Refrig.* 106 (2019) 133–143, <https://doi.org/10.1016/j.ijrefrig.2019.06.013>.
- [41] M. Yulianto, T. Suzuki, Z. Ge, T. Tsuchino, M. Urakawa, S. Taira, Y. Miyaoka, N. Giannetti, L. Li, K. Saito, Performance assessment of an R32 commercial heat pump water heater in different climates, *Sustain. Energy Technol. Assess.* 49 (2022), 101679, <https://doi.org/10.1016/j.seta.2021.101679>.
- [42] C. Yıldırım, D.B. Özkan, C. Onan, Theoretical study of R32 to replace R410A in variable refrigerant flow systems, *Int. J. Ambient Energy.* 39 (2018) 87–92, <https://doi.org/10.1080/01430750.2016.1269682>.
- [43] W. Li, Y. Zhang, L. Wang, H. Feng, T. Zhang, Evaluation of ionic liquid separation ability for the benzene–methanol mixture by extractive distillation, *J. Chem. Technol. Biotechnol.* 95 (2020) 1100–1109, <https://doi.org/10.1002/jctb.6294>.
- [44] E. Quijada-Maldonado, G.W. Meindersma, A.B. De Haan, Pilot plant study on the extractive distillation of toluene-methylcyclohexane mixtures using NMP and the ionic liquid [hmim][TCB] as solvents, *Sep. Purif. Technol.* 166 (2016) 196–204, <https://doi.org/10.1016/j.seppur.2016.04.041>.
- [45] K.R. Baca, G.M. Olsen, L. Matamoros Valenciano, M.G. Bennett, D.M. Haggard, B. J. Befort, A. Garcíadiego, A.W. Dowling, E.J. Maginn, M.B. Shiflett, Phase equilibria and diffusivities of HFC-32 and HFC-125 in ionic liquids for the separation of R-410A, *ACS Sustain. Chem. Eng.* 10 (2022) 816–830, <https://doi.org/10.1021/acssuschemeng.1c06252>.
- [46] A.R.C. Morais, A.N. Harders, K.R. Baca, G.M. Olsen, B.J. Befort, A.W. Dowling, E. J. Maginn, M.B. Shiflett, Phase equilibria, diffusivities, and equation of state modeling of HFC-32 and HFC-125 in imidazolium-based ionic liquids for the separation of R-410A, *Ind. Eng. Chem. Res.* 59 (2020) 18222–18235, <https://doi.org/10.1021/acs.iecr.0c02820>.
- [47] A. Garcíadiego, B.J. Befort, G. Franco, M. Mazumder, A.W. Dowling, What data are most valuable to screen ionic liquid entrainers for hydrofluorocarbon refrigerant reuse and recycling? *Ind. Eng. Chem. Res.* 61 (2022) 18412–18425, <https://doi.org/10.1021/acs.iecr.2c01928>.
- [48] P.J. Carvalho, T. Regueira, L.M.N.B.F. Santos, J. Fernandez, J.A.P. Coutinho, Effect of Water on the viscosities and densities of 1-butyl-3-methylimidazolium dicyanamide and 1-butyl-3-methylimidazolium tricyanomethane at atmospheric pressure, *J. Chem. Eng. Data.* 55 (2010) 645–652, <https://doi.org/10.1021/je900632q>.
- [49] J. Salgado, T. Regueira, L. Lugo, J. Vijande, J. Fernández, J. García, Density and viscosity of three (2,2,2-trifluoroethanol + 1-butyl-3-methylimidazolium) ionic liquid binary systems, *J. Chem. Thermodyn.* 70 (2014) 101–110, <https://doi.org/10.1016/j.jct.2013.10.027>.
- [50] C.M.S.S. Neves, K. Adi Kurnia, J.A.P. Coutinho, I.M. Marrucho, J.N. Canongia Lopes, M.G. Freire, L.P.N. Rebelo, Systematic study of the thermoophysical properties of imidazolium-based ionic liquids with cyano-functionalized anions, *J. Phys. Chem. B.* 117 (2013) 10271–10283, <https://doi.org/10.1021/jp405913b>.
- [51] M. Tariq, P.J. Carvalho, J.A.P. Coutinho, I.M. Marrucho, J.N.C. Lopes, L.P. N. Rebelo, Viscosity of (C2–C14) 1-alkyl-3-methylimidazolium bis(trifluoromethylsulfonyl)amide ionic liquids in an extended temperature range, *Fluid Phase Equilib.* 301 (2011) 22–32, <https://doi.org/10.1016/j.fluid.2010.10.018>.
- [52] Y. Zheng, Y. Zheng, Q. Wang, Z. Wang, Density, viscosity, and electrical conductivity of 1-Alkyl-3-methylimidazolium dicyanamide ionic liquids, *J. Chem. Eng. Data.* 66 (2021) 480–493, <https://doi.org/10.1021/acs.jced.0c00754>.

- [53] M.G. Freire, A. Rita, R. Teles, M.A.A. Rocha, B. Schröder, C.M.S.S. Neves, P. J. Carvalho, D.V. Evtuguin, L.M.N.B.F. Santos, J.A.P. Coutinho, Thermophysical characterization of ionic liquids able to dissolve biomass, *J. Chem. Eng. Data* 56 (2011) 4813–4822, <https://doi.org/10.1021/jc200790q>.
- [54] M.T.G. Jongmans, B. Schuur, A.B. De Haan, Ionic liquid screening for ethylbenzene/styrene separation by extractive distillation, *Ind. Eng. Chem. Res.* 50 (2011) 10800–10810, <https://doi.org/10.1021/ie2011627>.
- [55] Z. Zhu, Y. Ri, M. Li, H. Jia, Y. Wang, Y. Wang, Extractive distillation for ethanol dehydration using imidazolium-based ionic liquids as solvents, *Chem. Eng. Process. - Process Intensif.* 109 (2016) 190–198, <https://doi.org/10.1016/j.cep.2016.09.009>.
- [56] E.A. Finberg, T.L. May, M.B. Shiflett, Multicomponent refrigerant separation using extractive distillation with ionic liquids, *Ind. Eng. Chem. Res.* 61 (27) (2022) 9795–9812, <https://doi.org/10.1021/acs.iecr.2c00937>.
- [57] J. Li, T. Li, C. Peng, H. Liu, Extractive Distillation with ionic liquid entrainers for the separation of acetonitrile and water, *Ind. Eng. Chem. Res.* 58 (2019) 5602–5612, <https://doi.org/10.1021/acs.iecr.8b05907>.
- [58] S. Asensio-Delgado, D. Jovell, G. Zarca, A. Urriaga, F. Llovel, Thermodynamic and process modeling of the recovery of R410A compounds with ionic liquids, *Int. J. Refrig.* 118 (2020) 365–375, <https://doi.org/10.1016/j.ijrefrig.2020.04.013>.
- [59] P. Sridhar, J.D. Araujo, A.E. Rodrigues, Modeling of vanillin production in a structured bubble column reactor, *Catal. Today* 105 (2005) 574–581, <https://doi.org/10.1016/j.cattod.2005.06.044>.
- [60] J.L. Bravo, J.A. Rocha, J.R. Fair, Mass transfer in gauze packings, *Hydrocarb. Process.* 91 (1985).
- [61] R. Taylor, R. Krishna, *Multicomponent mass transfer*, John Wiley & Sons INC., 1952.
- [62] I. Díaz, J. Palomar, M. Rodríguez, J. de Riva, V. Ferro, E.J. González, Ionic liquids as entrainers for the separation of aromatic–aliphatic hydrocarbon mixtures by extractive distillation, *Chem. Eng. Res. Des.* 115 (2016) 382–393, <https://doi.org/10.1016/j.cherd.2016.07.012>.
- [63] N. Ramírez-Corona, N. Ek, A. Jiménez-Gutiérrez, A method for the design of distillation systems aided by ionic liquids, *Chem. Eng. Process. Process Intensif.* 87 (2015) 1–8, <https://doi.org/10.1016/j.cep.2014.10.016>.
- [64] H.H. Chen, M.K. Chen, B.C. Chen, L.L. Chien, Critical Assessment of Using an Ionic Liquid as Entrainer via Extractive Distillation, *Ind. Eng. Chem. Res.* 56 (2017) 7768–7782, <https://doi.org/10.1021/acs.iecr.7b01223>.
- [65] SULZER, Mellapak and MellapakPlus, (2022). <https://www.sulzer.com/en/shared/products/mellapak-and-mellapakplus> (accessed July 18, 2022).
- [66] Y. Chen, Z. Li, Y. Yang, J. Jia, C. Liu, M. Lucquiaud, Simulation of flooding phenomenon in packed column using electrical capacitance tomography, *IST 2019 - IEEE Int. Conf. Imaging Syst. Tech. Proc.* (2019), <https://doi.org/10.1109/ist48021.2019.9010204>.